Planck-scale gravity test at PETRA

Letter Of Intent

V.Gharibyan[*], K.Balewski

Deutsches Elektronen-Synchrotron DESY,

Notkestrasse 85, D-22603 Hamburg, Germany

Abstract

Quantum or torsion gravity models predict unusual properties of space-time at very short distances. In particular, near the Planck length, around $10^{-35}m$, empty space may behave as a crystal, singly or doubly refractive. This hypothesis, however, remains uncheckable for any direct measurement since the smallest distance accessible in experiment is about $10^{-19}m$ at the LHC. Here we propose a laboratory test to measure space birefringence or refractivity induced by gravity. A sensitivity $10^{-31}m$ for doubly and $10^{-28}m$ for singly refractive vacuum could be reached with PETRA 6 GeV beam exploring UV laser Compton scattering.

[*]Electronic address: vahagn.gharibyan@desy.de

Contents

1 Introduction

The quantum formalism can not be directly applied to gravitation and that is one of the major problems on a way of understanding and describing the physical reality. An important reason for this is the dynamical space concept adopted in general relativity, the currently accepted theory of gravity which states that any mass or particle modifies the space geometry (or metrics). On the other hand, the successful quantum theories within the Standard Model operate only in a fixed geometry space. For instance, observed violations of the discrete symmetries such as space, charge and time parities are attributed to the particles and their interactions while the scene of the interactions, the space-time, is considered to remain perfectly symmetric [1]. These two faces of space are believed to unify at distances near the Planck length $l_P = 1.6 \cdot 10^{-35} m$ (or mass $M_P = 1.2 \cdot 10^{19} GeV$, natural units are assumed throughout the letter). At this scale gravity is expected to be similar in strength to the electroweak and strong forces and quantum effects become important for the gravitational field. String theory and loop quantum gravity theory are prominent candidates which set a framework to make predictions in that energy domain. In many cases, unconventional space-time properties are suggested, such as vacuum refractivity [2] and/or birefringence [3].

Such effects may be studied by using lasers and high energy accelerator beams as recommended in ref. [4]. The proposed experiment at PETRA will probe the vacuum symmetry in a search for a handedness or chirality of the empty space presumed by quantum gravity. A figure of merit is circular birefringence $\Delta n = n_L - n_R$ of space, with $n_{L(R)}$ being the refraction index of left(right) helicity photons traversing the space. Average refraction $n = (n_L + n_R)/2$ will be tested with additional instrumentation.

In the following, quantitative theoretical estimates and existing experimental limits are quoted, the formalism of the suggested method is presented, and the proposed experimental setup is described. Expected performance, experimental reach with statistical and systematic accuracy estimates are discussed as well.

2 Photon dispersion at Planck-scale

Since Planck mass $M_P = \sqrt{c\hbar/G}$ is build from the speed of light and fundamental Planck and gravitational constants, this mass scale is considered to be relativistic and quantum gravitational. Most general modification of photon dispersion relation at lowest order of Planck mass could be expressed as

$$\omega^2 = k^2 \pm \xi \frac{k^3}{M_P} \tag{1}$$

where ω and k are photon's energy, momentum, respectively, while the ξ is a dimensionless parameter and the $\pm$ signs stand for opposite helicity photons. This is main relation we are going to test at PETRA.

Several theories are predicting or supporting the relation (1). The Planck scale quantum gravity modifies the Maxwell equations by adding extra terms proportional to the Planck length [5]:

$$\frac{\partial \vec{E}}{\partial t} = \vec{\nabla} \times \vec{B} - 2\xi l_P \vec{\nabla}^2 \vec{B} \tag{2}$$

$$\frac{\partial \vec{B}}{\partial t} = -\vec{\nabla} \times \vec{E} - 2\xi l_P \vec{\nabla}^2 \vec{E} \tag{3}$$

which leads to a deformed energy-momentum or dispersion relation (1). In the above equations, $\vec{E}$ and $\vec{B}$ describe the electromagnetic field. More general expressions accounting for space anisotropy are derived in Ref. [6]. Using conventional definition $n = d\omega/dk$, it is easy to verify that Eqs. (1)-(3) introduce a chiral vacuum with an energy dependent birefringence

$$\Delta n = 3 \cdot 10^{-19} \cdot \xi \cdot \omega[GeV] \tag{4}$$

where the magnitude of ξ defines the characteristic energies or distances where quantum-gravity effects become sizeable. In the simplest possible picture, this only happens at the Planck scale, and hence $\xi = 1$. However, the running of fundamental constants with energy may require quantum gravity to become active a few orders of magnitude below the Planck scale. The parameter ξ is there to account for such effects.

Another possible source of vacuum chirality is described by torsion gravity, an extension of the general relativity into the microscopic world to include particles' spins - for a review see [7]. In general, the spin gravity (space torsion) is considered to be weaker than the mass gravity (space curvature). However, near the Planck scale it may become detectable. Following Ref. [8], from the electromagnetic field Lagrangian

$$\mathcal{L} = -\frac{1}{4} F_{\mu\nu} F^{\mu\nu} + q T^{\mu\nu\rho} (\partial^\sigma F_{\mu\nu}) F_{\rho\sigma} \tag{5}$$

with a torsion tensor $T^{\mu\nu\rho}$ and free parameter q one derives a dispersion relation quite similar to Eq.(1)

$$\omega^2 = k^2 \pm q S_0 k^3 \tag{6}$$

where S_0 stands for a time component of the contorsion vector.

Myers and Pospelov [9] derived the expression (1) within effective field theory with dimension 5 operators. A similar effect is calculated in ref. [10] exploring graviton interaction with electromagnetic field in one-loop approximation. In our setup the gravitons emerge from the gravitational field of Earth. In summary, chiral space is a universal feature of Planck-scale gravity, in the sense that it is predicted by a large diversity of theories.

A nonbirefringent gravitational space is also possible and has been predicted within String theories using D-brane formalism. In Ref. [11] a polarization independent refractivity

$$n - 1 = \zeta \frac{k}{M_P} \tag{7}$$

is obtained for the space-time foam near the Planck length. Here we use ζ instead of the ξ to distinguish between the nonchiral and chiral space. In principle, both types may occur in the same vacuum at different scales ζ and ξ. Both gravity induced effects, namely birefringence and refractivity, share the common feature that their strength is growing with the photon energy. This is in contrast to the usual condensed matter or electromagnetic, nontrivial vacua where the refraction effects are suppressed by powers of the energy [12, 13]. Such growth should allow to approach Planck scale at the PETRA as will be shown below..

3 Current limits

Experimental limits on space chirality are set by astrophysical observations exploring birefringence induced depolarization of the linear light which comes from distant cosmological sources [14]. The limits, however, are based on assumptions about the origin, spatial or temporal distribution of the initial photons, and their possible interactions during the travel. Another critical assumption is a uniformly distributed birefringence over cosmological distances. The most stringent limit $\xi < 2.4 \cdot 10^{-15}$ is set by Ref. [15] based on photons with polarization 0.63 ± 0.30 in an energy range from 100 to 350 keV from GRB041219a [16]. Sensitive particle-physics effects have been suggested to test quantum gravity, mainly using threshold energies [17]. Applying cosmic ray constraints on photon decay and vacuum Cherenkov radiation [18], one arrives to $\zeta < 30$ and $\zeta < 300$ limits, respectively.

For the space refractivity, there are astrophysical observations interpreted [19] as $\zeta \sim 10$. This is derived from energy dependent time delay measurements of photons from distant sources. Similar to the results derived from polarized photons

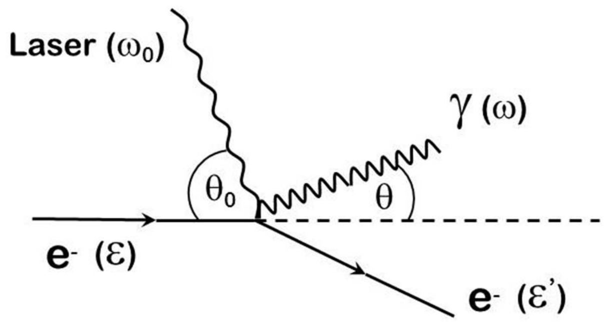

Figure 1: Compton scattering schematics.

of cosmological origin, strong assumptions have to be made on the source of these photons. In addition, quoted astrophysical constraints are valid only for photon-virtual graviton loop interactions, since the photon path is essentially free from gravitational fields.

PETRA measurements could shed light on the quantum-gravity promoted space chirality and refractivity including effects introduced by Earth gravitons. In the laboratory the Planck scale can be accessed by exploring the extreme sensitivity of the high energy Compton scattering to the vacuum refraction as discussed in the following.

4 Compton scattering affected by gravity

Let us denote by ω_0, ω, θ_0, θ the energies and angles of the incident and scattered photons relative to the initial electron direction as illustrated in Figure 1. Then, according to Ref. [18], for the high energy Compton scattering in a vacuum with $n \approx 1$ (up to $\mathcal{O}((n-1)^2)$ terms), the energy-momentum conservation yields

$$n - 1 = \frac{\mathcal{E}}{2\gamma^2(\mathcal{E} - \omega)} \left(1 + x + \theta^2\gamma^2 - x\frac{\mathcal{E}}{\omega} \right) \tag{8}$$

where γ,$\mathcal{E}$ are the Lorentz factor and energy of the initial electron, $x \equiv 4\gamma\omega_0 \sin^2(\theta_0/2)/m$, and n is the refraction index for the direction θ and energy ω. This formula is more general than Eq.(3) of Ref. [18]. The difference is in a factor $\mathcal{E}/(\mathcal{E} - \omega)$, because in contrast to [18] the final photon mass squared $k_\mu^2 = \omega^2(1 - n^2)$ is not neglected for this Letter.

Substituting $n-1$ in the Eq.(8) by the gravitational refractivity from the Eq.(7) we can estimate how the quantum gravity would change the scattered photons' maximal energy ω_m (Compton edge, at $\theta = 0$). The expected shift of the Compton edge is

$$\Delta\omega_m \equiv \omega_m(n) - \omega_m(1) = \frac{32\gamma^6\omega_0^2 \sin^4(\theta_0/2)}{(1+x)^4}\frac{\zeta}{M_P} \tag{9}$$

relative to the vacuum (n=1) kinematics. For optical lasers and head-on collision the kinematic factor $x \approx 2\cdot 10^{-5}\gamma$ and the right-hand side of Eq.(9) grows as γ^6 at GeV energies slowing down to γ^2 growth above TeV energies. At sufficiently high γ, the huge value of M_P is compensated and the energy shift becomes detectable. Hence, this effect allows quantum-gravity induced space refractivity to be measured at PETRA by laser Compton scattering off electrons with $\gamma = 11742$.

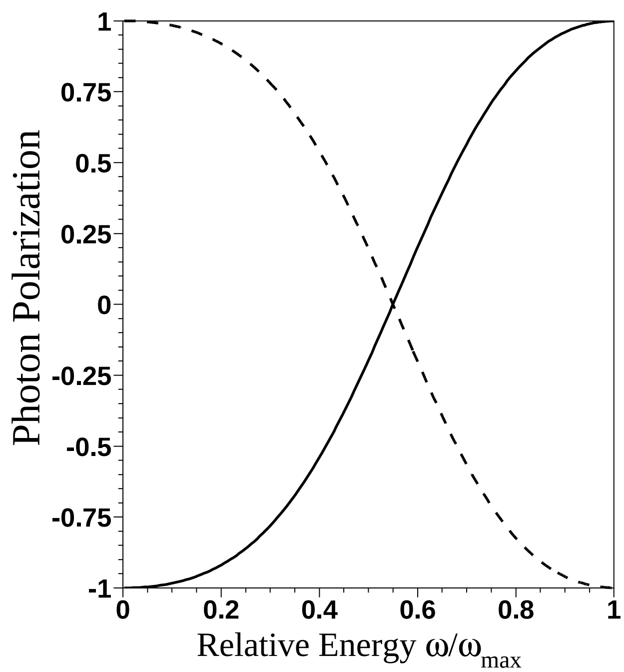

Figure 2: Polarization of the Compton scattered photon on a 6 GeV electron as a function of the photon energy. The solid and dotted lines correspond to the initial laser light helicity: +1 solid, -1 dotted.

In order to probe space birefringence, one needs to measure the refractivity in Eq.(8) for scattered photons of opposite helicity. This may be achieved by exploring circularly polarized initial laser beams and helicity conservation. The polarization of the secondary photons in the case of scattering on unpolarized electrons is shown in Fig. 2, using formulas from Ref. [20, 21]. At $\omega = \omega_m$ the polarization transfer is complete, such that the helicity of the Compton edge photons is fully defined by the laser light helicity. Consequently, in a birefringent vacuum the Compton edge energy is laser helicity dependent. Evaluating Eq.(8) for left and right helicity photons at $\theta = 0$ yields

$$\Delta n = n_L(\omega_m^L) - n_R(\omega_m^R) = \frac{(1+x)^2}{\gamma^2} A \tag{10}$$

where ω_m^L and ω_m^R are the highest energies for the Compton opposite helicity photons and
$A = (\omega_m^L - \omega_m^R)/(\omega_m^L + \omega_m^R)$ is an energy asymmetry.

Combining Eq.(10) with the gravitational birefringence from the Eq.(4) we arrive to

$$A = \frac{8\gamma^4 \omega_0 \sin^2(\theta_0/2)}{(1+x)^3} \frac{\xi}{M_P} \tag{11}$$

which proves that for PETRA values of γ the Planck scale space birefringence generates a measurable asymmetry.

In contrast to the astrophysical methods, an accelerator Compton experiment is sensitive to the local properties of space at the laser-electron interaction point and along the scattered photon direction. Hence, space isotropy tests are also possible as the accelerator rotates together with Earth. For any preferred direction the measured birefringence is expected to change as the scattered photon beam sweeps a circle over the celestial sphere. For a given direction (δ,α) of the photon beam and a possible anisotropy axis (δ_0,α_0) one expects

$$\Delta n = \Delta n_0 (\cos\delta \cos\delta_0 \cos(\alpha - \alpha_0) + \sin\delta \sin\delta_0) \tag{12}$$

where Δn_0 is the maximal birefringence, along the declination δ_0 and right ascension α_0. Despite of tight limits set by low energy high precision experiments on space anisotropy [22] the accelerator isotropy test is a valuable and complementary test at high energies.

5 Proposed experiment

In order to measure space birefringence and refractivity we propose a laser Compton experiment to be performed at the PETRA SW section. The experiment will

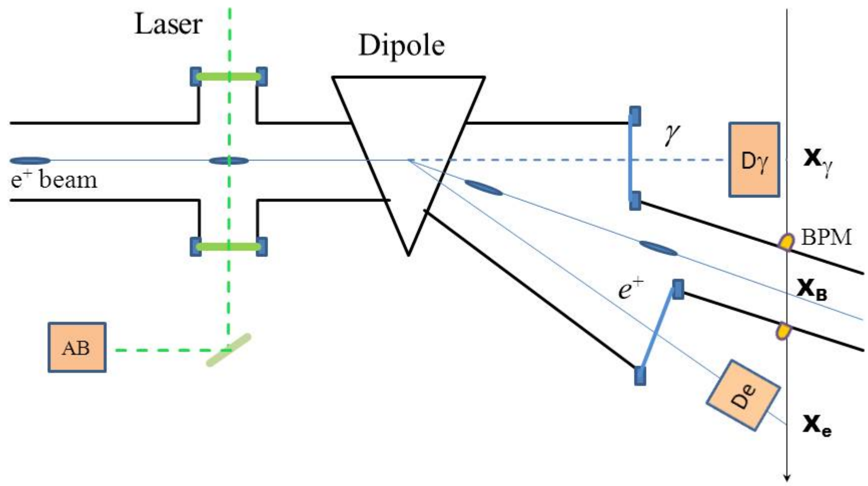

Figure 3: Schematic overview of the experiment.

bring into collision PETRA bunches and light pulses from a mode locked laser to produce Compton photons. Scattered photons and positrons, separated by a beam dipole magnet, are registered by downstream detectors. Positions and energies of the scattered secondaries will mainly be measured in single particle detection mode. Positron beam position is measured using PETRA high precision BPM (Beam Position Monitor) system [23]. Laser beam intensity and polarisation will be monitored in a light Analyzer Box. A schematic arrangement of the proposed experiment is presented in Figure 3. Measured positions X_e at laser light opposite helicities will allow to derive space birefringence while the refractivity could be accessed using in addition horizontal positions of the beam X_B and the Compton photon X_γ.

We plan to run the experiment in 'parasitic' mode without disturbing user operations or affecting machine beam quality.

5.1 Accelerator

PETRA III [24] is a third generation light source with 6 GeV high quality positron beam. Main operational parameters of the machine [25] are collected in the table 1.

Time resolved state with 40 or 60 bunches is the main working mode of the machine. Top-up running allows long-term stable operation with constant current. On Figure 4 a typical performance of the PETRA is shown over a 24 hours period.

Table 1: PETRA III parameters.

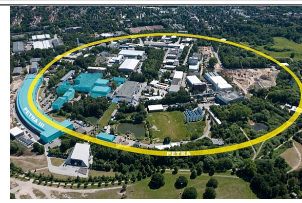	
Positron energy	6.0 GeV
Circumference of the storage ring	2304 m
Harmonic number (buckets)	3840
Number of bunches	40 – 960
Bunch separation	192 ns – 8 ns
Positron beam current	100 mA (top-up mode)
Horizontal emittance	1 $nm \cdot rad$ (rms)
Vertical emittance	0.01 $nm \cdot rad$ (rms)
Positron beam energy spread	0.1% (rms)
RF	499.564 MHz
Revolution Time	7.685 μsec
Revolution Frequency	130.121 kHz
Bunch Length (rms)	44 psec
Positron Energy Loss per Turn from Dipoles	1 MeV
Overall Positron Energy Loss per Turn	6 MeV
Positron Beam Lifetime (Time resolved Mode)	2 h

At the planned laser-positron interaction point PETRA beam has a horizontal dispersion $D_x = 0.139m$ and following Twiss parameters
$\alpha_x = 0.427$, $\beta_x = 11.114m$
$\alpha_y = -1.311$, $\beta_y = 19.945m$
with RMS beam sizes $\sigma_x = 106\mu m$ and $\sigma_y = 24\mu m$
and RMS divergences $\sigma_{x'} = 10\mu rad$ and $\sigma_{y'} = 2\mu rad$.

5.2 Laser

Laser in this application should provide sufficient luminosity for high Compton rates at single or few particles operational mode. In addition the light wavelength should

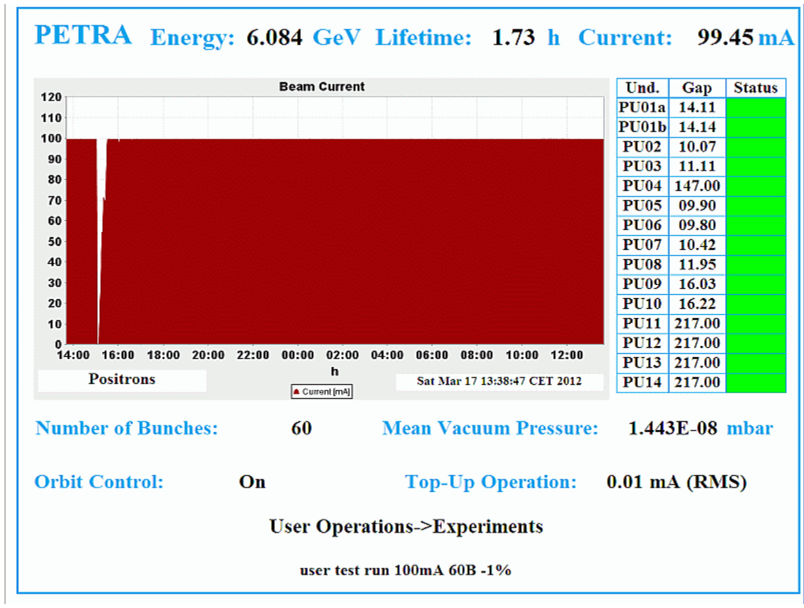

Figure 4: PETRA online status dysplay [26].

be possibly short to extract and detect the scattered positrons within available limited distance from interaction point. These two requirements somewhat contradict each other since the Compton cross-section is falling toward shorter wavelengths. Thus, at acceptable wavelengths the laser power demand is so high that appropriate CW lasers are not available in market. Since high power Q-switched lasers are not adequate for single particle mode applications, we have to choose among mode-locked lasers. An example of commercially available laser which meets our needs is Coherent Paladin UV laser [27] with parameters listed in the table 2.

The laser light will be delivered to the interaction chamber by a single mode, polarization maintaining fiber. This will provide fixed position of the light at the interaction point independent of the polarization state. At the end of the fiber a quarter wave plate will convert linear light into a circular one which then will be focused $< 10\mu m$ to the positron beam. Polarization state of the interacting laser photons will be controlled by an electro-optical Pockels-cell device installed upstream of the fiber. Light polarization and intensity will be constantly monitored at laser beam dump, in Analyzer Box.

Table 2: Coherent Paladin laser specifications.

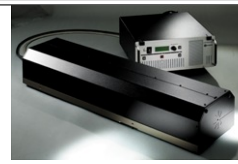

Wavelength	355 nm
Output Power	> 8 W
Repetition Rate	80 ± 1 MHz
Pulse Length	> 15 ps at 1064 nm
Spatial Mode	TEM00
M2	< 1.2
Beam Diameter	$1 \pm 15\%$ mm
Beam Divergence	$< 550\mu rad$
Beam Ellipticity	0.9 to 1.1
Pointing Stability	$< 20\mu rad/^{\circ}C$
Polarization linear	$>$ 100:1, vertical
Long-term Power Stability	$< \pm 2\%$

5.3 Experimental sensitivity

Given the accelerator energy of 6 GeV, laser wavelength of 355 nm and $e\gamma$ crossing angle of 90°, gravity induced effects could be calculated using Eq.(9) and Eq.(11). Single refraction in crystal space will shift the Compton edge while laser helicity flip will produce an energy asymmetry induced by double refraction. Magnitude of these effects are shown in Figure 5. Experimental reach of the experiment is then defined by accuracies for the energy and asymmetry measurements as well as limiting systematic effects. We expect precisions of $\Delta\omega_m/\omega_m = 10^{-3}$ to 10^{-4} for energy and 10^{-7} to 10^{-8} for asymmetry measurements which are corresponding to upper right and lower left regions on the Figure 5. Detailed calculations will be presented in the folowing sections.

5.4 Beamline

We plan to use existing beamline and interaction vacuum chamber build for PETRA-III Laser-Wire project [28] (see Figure 6). The chamber has horizontal and vertical

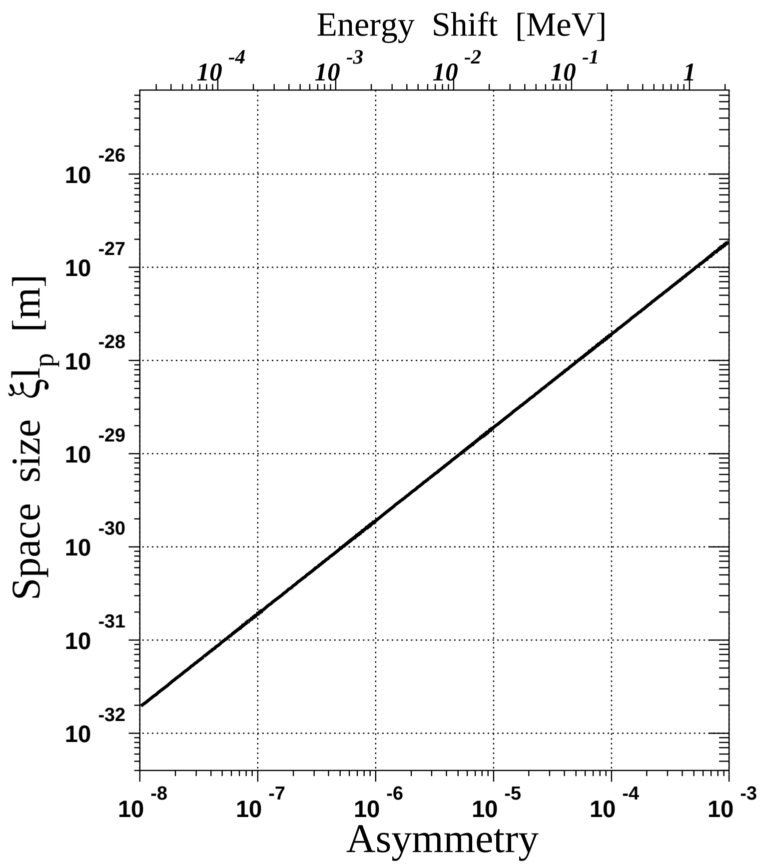

Figure 5: Sensitivity of the PETRA III for vacuum birefringence and refractivity. Birefringence at the scale ξ will produce a Compton edge asymmetry (lower scale) while the refractivity produces absolute energy shifts (upper scale).

optical entry-exit ports (windows) for the laser. For our application we will use vertical ports which assumes careful stress-less mounting of the laser windows to preserve circular polarization of the light.

A vacuum exit window (2mm Al) for the Compton photons is located at 7.8m distance from the interaction chamber. Beamline essential components are listed in table 3 and are drawn in Figure 7.

Beam position monitors (BPM) near and around the interaction point are dedicated for beam position, slope (BPM-SL1, BPM-SL2) and bunch timing (Pickup) measurements [29]. Beam horizontal position evaluated by BPM-X_B at SWL 0.6m

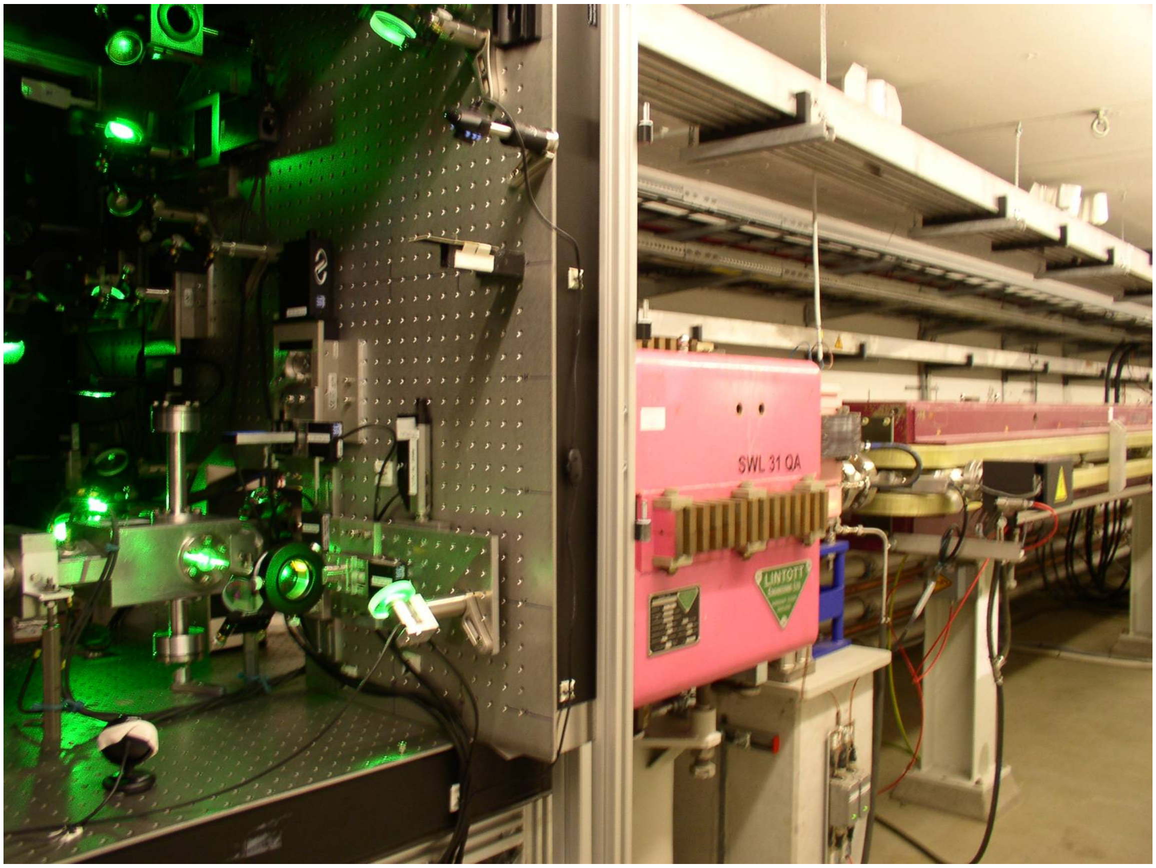

Figure 6: Existing beamline: interaction chamber surrounded by Laser-Wire optics with following quadrupole and dipole magnets. A green laser is shining through horizontal view port of the chamber.

will enter space refractivity derivations.

Most important beamline element, apart the interaction chamber, is a 5.4m dipole which will separate scattered positrons and photons from the PETRA (neutral) beam. Focusing and defocusing quadrupoles are assigned by $Q+$ and $Q-$ respectively, relative to the horizontal (x) plane. Quadrupoles located downstream of the dipole will noticeably bend the Compton edge positrons because of considerable horizontal offsets from the quadrupole center. Such a bend is visible at the last defocusing quadrupole in the Figure 7. Last focusing quadrupole bend should be compensated to achieve necessary separation between the extracted positron and neutral beam at the exit window. Characteristics of the dipole and quadrupole mag-

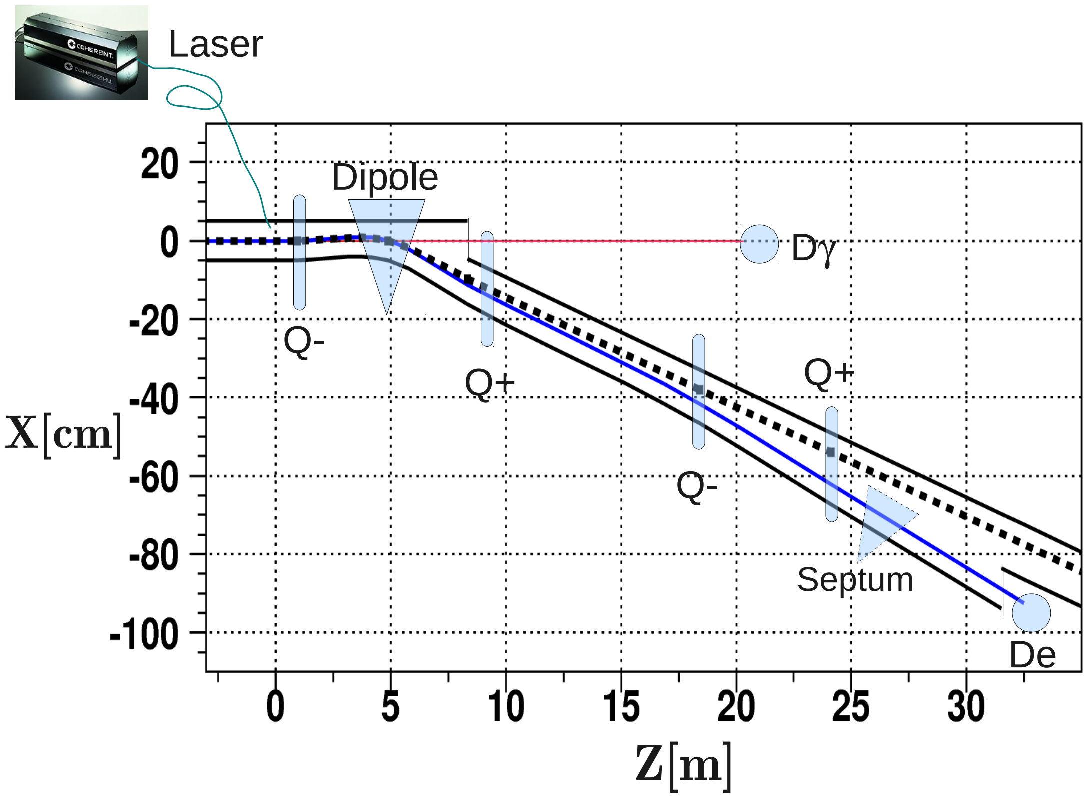

Figure 7: Beamline elements relative to laser and positron beam (dotted line) interaction point ($Z = 0m$, $X = 0cm$). Beam pipe and exit windows are drawn in black, trajectories for Compton edge positrons and photons are shown in blue and red. Q(-)+ are assigned to (de)focusing quadrupoles. Photon and electron detectors denoted by $D\gamma$ and De respectively.

nets [25] are displayed in table 4 for the 6 GeV machine and nominal beam optics conditions.

Separations between neutral beam and scattered photons and positrons are also included in the table 3 (last 2 columns). These distances are calculated at the geometrical centers of the magnets along z. Table shows sufficient outside (the ring) room to place a γ detector starting about 25m downstream of the interaction point while the Compton positrons could be comfortably detected at 31.5m, inside the ring.

Table 3: Positions of beamline components.

Component name	DB name	Position SWL(m)	Position vs IP(m)	$\gamma - e$ beam separation $X_B - X_\gamma$ (cm)	$e' - e$ beam separation $X_e - X_B$ (cm)
BPM-SL1	BPM	38.8295	-6.5055		
BPM-SL2	BPM	32.6000	-0.2760		
IP	LSW	32.3240	0.0000	0.0000	0.0000
Q-	Q5K	31.3670	0.9570	0.0000	0.0000
Pickup	BPM	30.9365	1.3875	0.0000	0.0000
Dipole	DK	27.4410	4.8830	4.8288	0.7745
Q+	Q4K	23.9980	8.3260	9.6576	1.5489
Q-	Q2K	13.9000	18.4240	37.9824	3.6515
Q+	Q1K	8.2000	24.1240	53.9708	8.2569
BPM-X_B	BPM	0.6000	31.724		
e-window	-	0.8240	31.8500	74.6604	14.2165

Vacuum beam pipe downstream of the Q2K should be modified to allow extraction and detection of the Compton scattered positrons. For that the vacuum pipe has to be extended on inner side as it seen on the Figure 7. The extension will end by a Titanium exit window of thickness $356\mu m$ and size $60mm \times 20mm$. In addition magnetic field of the last quadrupole Q1K should be shielded for scattered positrons. Otherwise focusing field of the quadrupole is considerably strong for off-center Compton edge positrons to bring them back to the beam. In case of technical difficulties for quadrupole field shielding, it is possible to use an additional dipole magnet. Right after the Q1K quadrupole there is sufficient separation (about 7 cm) between the Compton positrons and neutral beam to accommodate a septum magnet.

In contrast to space birefringence, experiment for the refractivity requires absolute position measurements of the scattered Compton particles. Therefor, positioning and alignment of the γ, e^+ detectors and the laser beam should be done with best available accuracy in horizontal plane. For absolute calibration of the BPM-XB a horizontal wire scanner should be installed in near vicinity of the BPM.

Table 4: Magnet parameters.

Dipole	
Length	5.378 m
Bending angle	1.607°
Bending radius	191.73 m
Field	0.10439 T
Field Error $\Delta B/B$	$5 \cdot 10^{-4}$
Critical Energy	2.499 keV
Quadrupoles	
Length	1042 mm
Aperture	50 mm
Gradient (max)	15 T/m
k	$0.749 m^{-2}$
Field Error $\Delta k/k$	$4 \cdot 10^{-3}$

6 Expected performance

6.1 Compton spectra

For 6 GeV PETRA and 355 nm laser, energy and angular distributions of the Compton positrons and photons are presented on Figure 8. Scattering kinematic factor is x=0.16 which corresponds to Compton edge positron (minimal) energy of $\mathcal{E}'_{min} = 5.17\ GeV$. At this energy the scattered positron retains initial movement direction as it is clear from the plot displaying angular dependencies. Compton edge photons follow the same direction with an energy of 0.83 GeV.

Hunted gravitational effects will change energy sharing between the positron and photon. Expected changes are relatively small and will be hardly detectable by direct calorimetry so, we will use beamline magnets to convert scattered positron energy (momentum) to position in order to explore more sensitive instrumentation. To estimate spatial relationships we apply an approximate formula connecting energy and position of the scattered positron. Detected horizontal position of the scattered positron with energy $\mathcal{E}'$ could be presented by

$$X = X_0 + (Z - Z_D)\left(\theta_x + \frac{eLB}{\mathcal{E}'}\right) \tag{13}$$

where X_0, θ_x are position and horizontal angle of the positron at the laser interac-

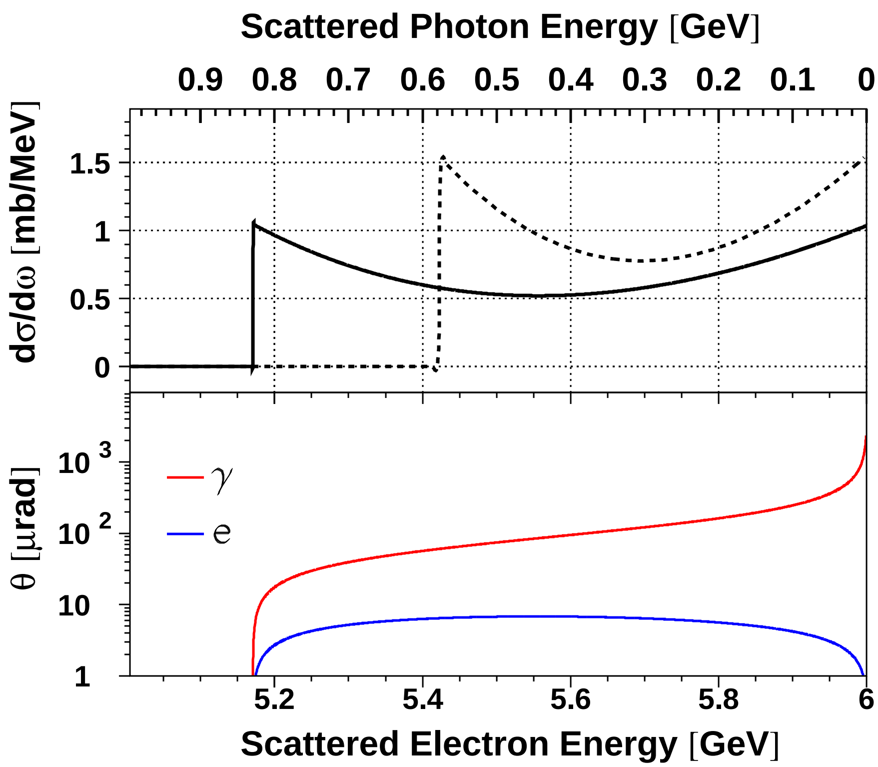

Figure 8: Compton cross-section and scattering angles for initial 6 GeV positron and 3.49 eV photon. Laser and e^+ beam crossing angle is 90°. Dotted line spectrum is for 2.33 eV green laser.

tion point, Z and Z_D are locations of the detector and bending dipole respectively. Here L and B stand for the dipole length and magnetic field while influence of the quadrupoles is ignored. From this relation it follows that an energy change $\Delta\mathcal{E}'$ around the Compton edge will produce a position change

$$\Delta X = 144.3\Delta\mathcal{E}'\mu m/MeV$$

at the detector location Z=32m.

6.2 Smearing factors

Momentums and energies of Compton particles are smeared by initial laser and positron beam position, angular and energy distributions. We use Eq.13 with e^+

beam optics parameters and numbers from Table 1, Table 2 to calculate magnitudes of smearing factors. Estimated influence of different factors on position of the Compton edge positron at detector location is shown in Table 5.

Table 5: Smearing factors.

Factor	Value	$\mathcal{E}'$ smearing
e^+-laser IP	$\sigma_{IPx} = 10\mu m$	$10\mu m$
e^+ energy spread	$\sigma_{\mathcal{E}}/\mathcal{E} = 10^{-3}$	$750\mu m$
e^+ divergence	$\sigma_{x'} = 10\mu rad$	$280\mu m$
e-window	$\sigma_{Mult} = 2.4mrad$	$50\mu m$

Apart from the mentioned main contributing factors Table 5 displays also smearing by multiple scattering in the positron exit window. Overall smearing is about $800\mu m$ which agrees to a detailed simulation results presented in Figure 9. Dominant smearing contributor is the lepton beam energy spread, quantifying as $\sigma_{x\mathcal{E}} \approx \Delta X_{ee'}\sigma_{\mathcal{E}}/\mathcal{E}$ with $\Delta X_{ee'}$ being separation between scattered positron and neutral beam at detector location. Hence, one can reduce smearing induced by inter-bunch energy spread only via moving detector closer to IP with an expense of shrinking available place for the e' detectors.

6.3 Rates

Compton secondaries will be detected in single particle resolving regime with about 0.01 particles per bunch. PETRA mostly operates with 40, 60 or 240 bunches [30] with corresponding inter-bunch spacings of 192ns, 128ns and 32ns. Therefor, expected Compton rates are 52kHz, 78kHz and 313kHz for different bunch modes of the machine. However, since we are interested exceptionally on the Compton edge particles, the rates can further be reduced by discriminating energies of the photons or positrons. Assuming 5% energy detection resolution for single particles the rates could be reduced by a factor of 3 or 12 triggering on the positron or photon calorimeter respectively. This numbers are derived by integrating spectrum on the Figure 8 within ranges of 0 to 100% and 95% to 100%.

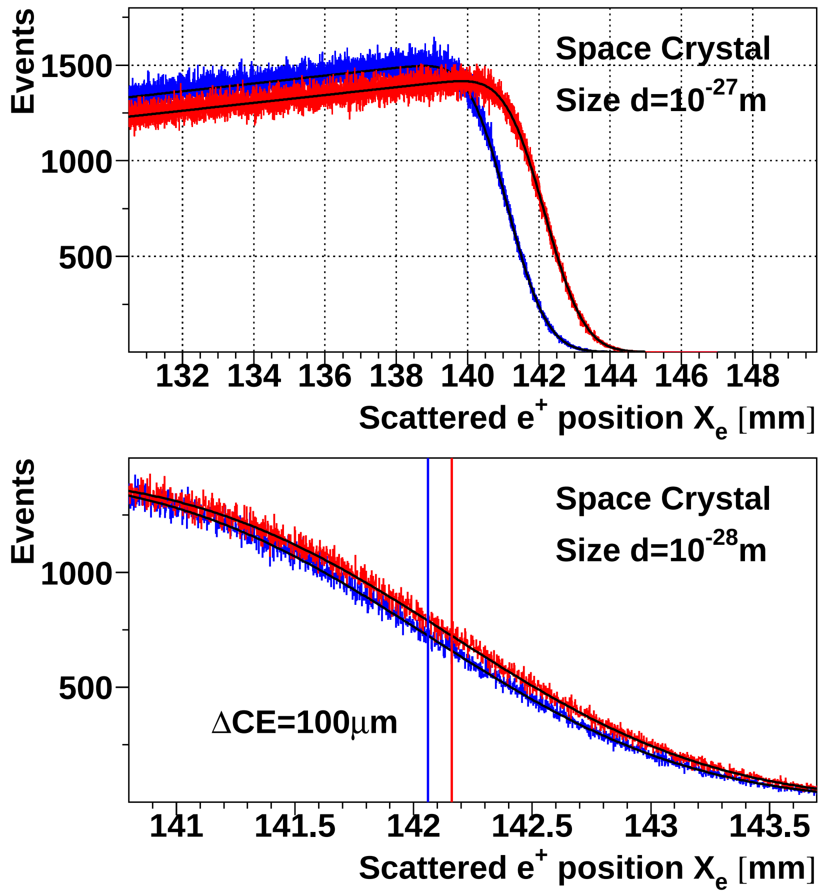

Figure 9: Simulation results: scattered positron spatial spectra for laser left and right helicities. Horizontal scale is distance between the scattered e^+ and neutral beam at the detector location. Lower plot shows Compton Edge (CE) positions obtained by fitting a 4 parameter function from ref. [36] to spectra. Same function is applied for fitting upper plot distributions.

6.4 Detectors

In previous sections we have defined energy and rate of the expected signals. For e^+ and γ produced at Compton edge, simultaneous position and energy measurements are necessary. We intend to install a combination of position sensitive and calorimetric detectors at the positron and photon branch. For energy measurements homogeneous crystal calorimeters could provide a resolution of 5% over $\sqrt{\mathcal{E}}$. Posi-

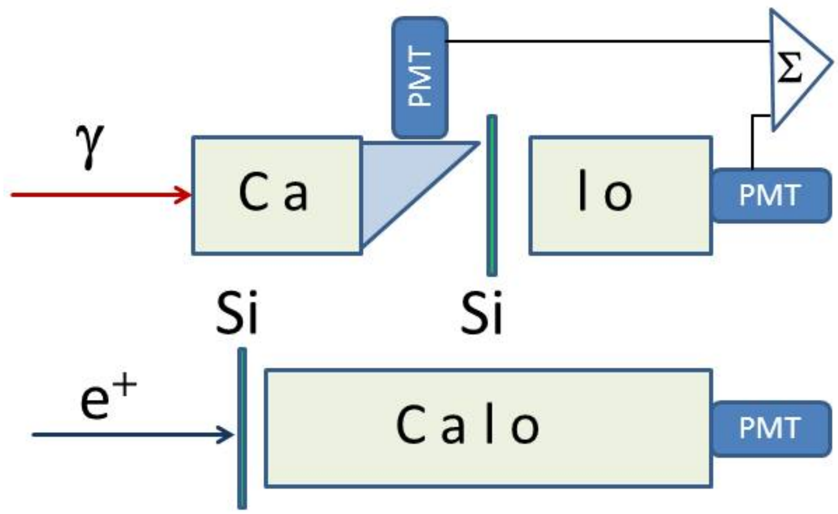

Figure 10: Photon and positron detectors schematics. Position sensitive part is denoted by "Si" and energy sensitive part by "Calo". PMT stands for photomultiplier.

tion measurements will be performed with silicon strip or pixel detectors. A position resolution of $10\mu m$ and rate capability of 30 kHz would be sufficient for the whole range of our measurements. The silicon detector will be placed in front of calorimeter for positrons while for the photons position detector will be located at middle part of the calorimeter where shower lateral size is maximal. This arrangement is displayed in Figure 10.

6.5 Backgrounds

Apart from the laser Compton scattering there are other beam related sources of scattered photons or leptons at any accelerator environment. These particles may enter detectors and spoil measured distributions. For storage rings one should first consider synchrotron radiation from bending or quadrupole magnets [31]. In our case positron detectors are located inside the ring and could see only scattered synchrotron light while the ouside photon detectors are imposed to direct synchrotron radiation. Therefor we plan to shield detectors at the beam pipe side and, in addition, the photon detectors also at the front side to absorb completely the synchrotron radiation.

Other potentially dangerous processes are beam-gas interaction [32], scattered blackbody radiation [33, 34] and intra-bunch scattered (Touschek) positrons [35]. Explored positron and photon coincidence registration mode will greatly suppress or completely eliminate backgrounds from the thermal photons and Touschek positrons. The beam-gas Bremsstrahlung, however, can not be discriminated since the energy balance is similar to the Compton scattering. This would be the main background and it should be handled by keeping vacuum pressure around the Compton interaction point possibly low (mounting of additional vacuum pumps should be foreseen). The Bremsstrahlung rate will be monitored periodically by blocking the laser light by a shutter. Alternatively a fast, electro-optical or acousto-optical modulator may be used to redirect the laser out of certain portion of bunches for background measurements.

A more severe source of background at the SW section could be aperture limitations - beam collimators (coll1 and coll2) of PETRA are located about 15m upstream and downstream of our detectors.

6.6 Measurements

6.6.1 Space birefringence

As it was described above for space chirality measurements the laser helicity will be flipped with few hundred Hertz sweeping frequency to avoid correlations with any possible periodic source. Accumulated spatial events will be tagged with the helicity and the resulted spectra (simulated samples are shown on Figure 9) will be analyzed to fetch the Compton edge for each helicity. For that the spectra could be fitted by gaussian and error combined functions as it is proposed in [36] or by Compton cross-section convoluted with detector resolution, as in [18]. An example of fitted spectra is shown in Figure 9, where a Compton edge shift of $100\mu m$ is detected by fits for simulated initial space birefringence at $\xi = 10^7$ $(\approx 10^{-28} m)$. After the fits an asymmetry

$$A = \frac{{X_e}^+ - {X_e}^-}{{X_e}^+ + {X_e}^-} \tag{14}$$

will be calculated with ${X_e}^+$, ${X_e}^-$ being Compton edge positions for positive and negative helicities. Finally, this measured asymmetry will be related to Eq.(11).

6.6.2 Space refractivity

For vacuum index measurement it is necessary to detect absolute energy of the Compton edge positron or photon. This could be accomplished by simultaneous measurements of the photon X_γ, positron X_e, and neutral beam X_B positions [1] (see Figure 3). With this information one can use Eq.(8) and Eq.(13) to arrive to

$$n - 1 = \frac{1}{2\gamma^2}\left(x\frac{(X_B - X_\gamma)^2}{(X_e - X_B)(X_e - X_\gamma)} - 1\right) \tag{15}$$

which holds if the scattered positron and the neutral beam are transported through the same (strength) magnetic field, i.e. for homogeneous dipole field. With quadrupoles one needs to apply corrections which could be measured during calibrating quadrupole scans. This is, still, not the full story, since any small offset in beam energy value $\mathcal{E}_{beam}$ would result in a fake refractivity measurement. Therefor, for space refractivity experiment it is necessary an independent, precise measurement of the beam absolute energy. Moreover, since the beam energy changes along the ring, the energy measurement should be done at the Compton interaction point. For this we will explore a different frequency light generated by the same or another laser. Since the UV 355nm light is third harmonic of the 1064nm Nd:YAG laser, we can use second harmonic, 532nm wavelength which otherwise is widely available as a standalone laser solution.

Combining Eq.(8),(7) and Eq.(13) for two laser photon energies, after some lengthy though simple calculations we obtain expressions for beam energy and refractive space size measurements

$$\mathcal{E}_{beam}\,[GeV] = \frac{u_1 + u_2L_2 + u_3L_1 + u_4L_1L_2}{u_5 + u_6L_2 + u_7L_1 + u_8L_1L_2} \tag{16}$$

$$\zeta l_P\,[m] = 7\cdot 10^{-24}\frac{v_1 + v_2L_2 + v_3L_1 + v_4L_1L_2 + v_5L_1^2 + v_6L_1^2L_2}{v_7 + v_8L_2 + v_9L_1 + v_{10}L_1L_2 + v_{11}L_1^2 + v_{12}L_1^2L_2} \tag{17}$$

where L_1, L_2 are incorporating position measurements for the laser 1 (UV, 3.49 eV) and laser 2 (green, 2.33 eV) and

$$L = \frac{X_e - X_B}{X_B - X_\gamma} \tag{18}$$

is a common expression to calculate L_1, L_2. Coefficients u and v depend solely on two laser wavelengths, crossing angles and a central energy of e^+ beam chosen to be $\mathcal{E}_0 = 6.00000\ GeV$. Resulting expressions are too long to be presented here, hence we display numerical values of the coefficients in Table 6.

[1]Method is similar to a 3-positions measurement scheme proposed for ILC energy determination [37].

Table 6: Coefficients in Eq.(16) and Eq.(17).

$u_1 = 0.03747513690$	$u_2 = -8.245513915$
$u_3 = 3.281272436$	$u_4 = -5.001716619$
$u_5 = -0.04417775880$	$u_6 = 0.8269285477$
$u_7 = -0.7135896078$	$u_8 = 0.1575166987$
$v_1 = 0.00100246550$	$v_2 = -0.2205687272$
$v_3 = 0.1319522859$	$v_4 = -0.9607252134$
$v_5 = 0.7135896078$	$v_6 = -0.1575166987$
$v_7 = -0.04417775880$	$v_8 = 0.8269285477$
$v_9 = -0.7577673666$	$v_{10} = 0.9844452464$
$v_{11} = -0.7135896078$	$v_{12} = 0.1575166987$

Described formalism allows to measure space refractivity provided UV and green lasers to be delivered to the same interaction point. Spatial separation of Compton edge positrons from two lasers will be 40.915 mm thus allowing to use the same exit window and e^+ detector.

6.6.3 Space anisotropy

Possible spatial dependence of space birefringence or refractivity will be tested by writing Eq.(12) for PETRA declination angle $\delta = 22.58^\circ$ at interaction point

$$Q = Q_0(0.92 \cos \delta_0 \cos(\alpha - \alpha_0) + 0.38 \sin \delta_0) \tag{19}$$

with $Q = \Delta n$ for measured birefringence or $Q = n - 1$ for refractivity. For each measurement time a corresponding right ascension angle α will be calculated and obtained $Q - \alpha$ dependence will be fitted by Eq.(19) to find space anisotropy axis direction δ_0, α_0.

7 Experimental reach and accuracy

7.1 Statistical errors

For an expected small asymmetry from Eq.(14) ${X_e}^+ \approx {X_e}^- = X_e \approx 142mm$, error propagation gives

$$\Delta A = \frac{1}{\sqrt{2}} \frac{\Delta X_e}{X_e} \tag{20}$$

where ΔX_e is accuracy of the Compton edge (X_e) measurement. Although Compton edge is derived by fitting distribution with many events, for statistical error estimation it is more convenient evaluating a single event accuracy which allows a direct application of conventional statistical events-strength formalism. Thus, we can assign $\sigma_{X_e} \approx 800\mu m$ as position error for a single event equal to the position smearing derived above, and get $\Delta X_e = \sigma_{X_e}/\sqrt{TR_e}$, where R_e is rate of e^+ events around Compton edge and T is time of measurement. Necessary data taking times to achieve different sensitivities, for an average rate of $R_e = 13kHz$ (estimated from 2011 running [30]), are displayed on Table 7.

Table 7: Asymmetry measurement times and space birefringence sensitivities.

ΔA	ξl_P	T
10^{-5}	10^{-28}m	12 sec
10^{-6}	10^{-29}m	20 min
10^{-7}	10^{-30}m	34 hours
10^{-8}	10^{-31}m	141 days

On a way to calculate refractivity measurement errors we estimate spreads of Eq.(18) constituents. A Compton photon position at detector location, X_γ, defines initial angle θ_x. Hence, the difference $X_e - X_\gamma$ will be free from fluctuations of the θ_x. The beam position X_B is a measure of magnetic field strength which is completely defined if we explore beam direction (slope) at the interaction point, measured by two upstream BPMs. From BPM resolution of $5\mu m$ per bunch traverse [38] we arrive to following accuracy estimators for a Compton scattering event:
$\sigma(X_\gamma) = 20\mu m$
$\sigma(X_B) = 15\mu m$
$\sigma(X_e) = 752\mu m$

the latter is a quadratic sum of smearings by beam energy and exit window from the Table 5. Error propagation applied to Eq.(17), with derived numbers, yields an accuracy of $5 \cdot 10^{-26}m$ for ζl_P from two (UV and green) Compton edge scattering events. Evaluating Eq.(16) with the same events we find a 300 MeV statistical error for $\mathcal{E}_{beam}$. At PETRA this would apply 50 sec data taking time at 5 kHz for beam energy measurement with a 10^{-3} relative statistical error. A sensitivity of $10^{-28}m$ for space refractivity will be achieved during the same time period.

7.2 Systematic effects

7.2.1 Space birefringence

In general, it is a difficult task to mention asymmetry limiting sources a priori since most (theoretically all) of beam and detector parameters and their drifts are not (should not be) affected by helicity flips and are ignorable for asymmetries. Therefor, we refer to asymmetry measurement achievements of former accelerator experiments. Asymmetries as small as 10^{-7} have been detected with a sensitivity 10^{-8} at the SLAC 50 GeV experiments [39, 40], based on beam helicity flips. Same order sensitivities for measured asymmetries are reported at the MAMI 1 GeV experiments [41, 42]. Thus, similar accuracies seem reachable at PETRA which suggests that the 6 GeV machine could test space birefringence down to $10^{-31}m$.

There are few potential sources of false asymmetry which are correlated with laser helicity flips and are all related to either the laser or lepton beam polarization. These are positron beam longitudinal or transverse polarization and laser light linear polarization. Introduced asymmetries by the mentioned factors, for 100% polarization, are plotted on Figure 11. First we note that none of the quoted factors could shift the Compton edge, although, intensity changes displayed on the Figure 11, convoluted with detectors responses, could mimic a shift of the edge. However, positron beam longitudinal polarization in PETRA should be plain zero - otherwise the proposed setup is able to measure and monitor even small amounts of it. Situation is different for the circular laser light where always a small fraction of linear component exist [43] and for the PETRA beam transverse polarization which could be acquired by Sokolov-Ternov mechanism [44]. Nevertheless, since intensity changes produced by helicity flips are vanishing at the Compton edge, contribution of these two factors to gravitation induced asymmetry should be negligible.

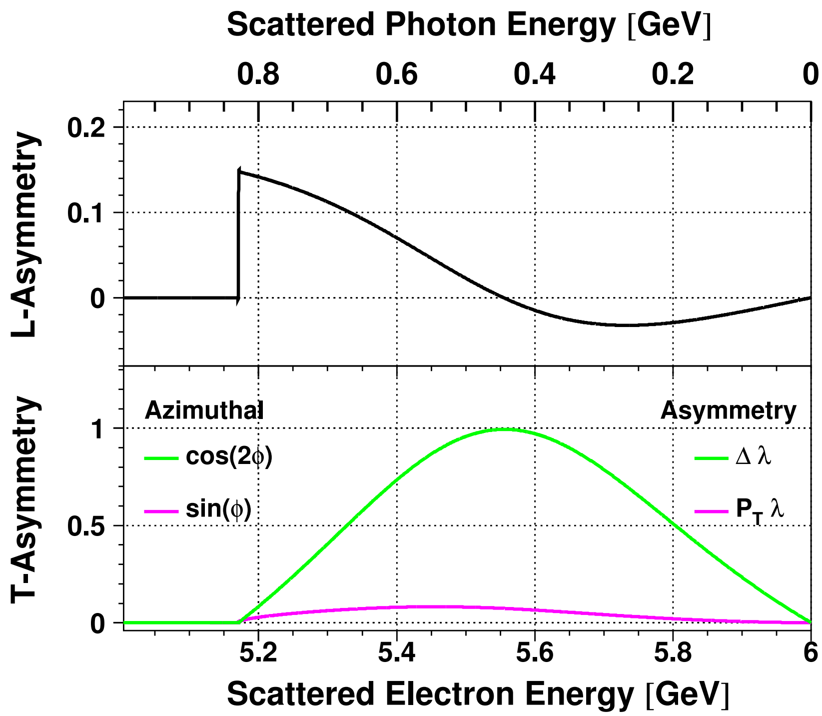

Figure 11: Compton cross-section asymmetry produced by laser helicity flip. Upper plot: for longitudinal positrons. Lower plot: for transversal (magenta) or unpolarized (green) positrons. In latter case laser polarization is linear.

7.2.2 Space refractivity

Limiting factor for refractivity measurement is positron beam energy uncertainty $\Delta\mathcal{E}$. We can calculate corresponding effect on refractivity measurement using Eq.(8) by explicitly writing γ and x dependence on $\mathcal{E}$ at the Compton edge. Resulting expression

$$\Delta(n-1) = \frac{1}{2\gamma^2}\frac{\Delta\mathcal{E}}{\mathcal{E}} \tag{21}$$

sets an accuracy limit for refractivity measurement with the proposed method. With $\Delta\mathcal{E}/\mathcal{E} \approx 10^{-3}$ a systematic error for refractivity is $3.6 \cdot 10^{-12}$ which corresponds to $\zeta = 7.3 \cdot 10^6$ and an experimental reach to space crystal size of $1.2 \cdot 10^{-28} m$. Bending field inhomogeneity should contribute twice as less as energy spread since it enters to Eq.(13) together with the energy and has $5 \cdot 10^{-4}$ relative uncertainty.

8 Cost estimate

Since most of hardware should be adapted to existing beamline and magnets, there are no standard components available and therefor, we can only roughly estimate amount of necessary expenses. Our estimates are shown in Table 8.

Table 8: Equipment expenses.

Component	Cost (kEuro)
Laser system	250
Beam pipe	75
Septum magnet	75
Detectors	150
Total	550 kEuro

Prices for optics and electronics are included in laser and detector costs respectively.

9 Conclusion

A simple theoretical framework is established allowing to access extremely small distances in laboratory, provided a vacuum refraction index growing with photon energy. Such vacuum is suggested by wide range of gravity theories which predict space-time modifications around Planck scale. Motivated by these predictions, we propose a laser Compton experiment at PETRA to test empty space for single or double refraction. Experiment would be able to prove or reject crystal-space hypothesis reaching distances as small as $10^{-28}m$ for refractivity and $10^{-31}m$ for birefringence. Space isotropy measurements within these magnitudes are also foreseen.

Space birefringence measurements would be performed with UV polarized laser and would require 282 days of data taking (50% efficiency assumed) to reach $10^{-31}m$ sensitivity. Probing space isotropy within this running period is possible with a sensitivity $10^{-30}m$ by mapping 360° celestial circle with 3.6° steps.

For space refractivity tests one should explore an additional green laser which will enable beam energy precise determination. Very fast, sub-minute measurement times are sufficient to sample refractivity with an accuracy which corresponds to $10^{-28}m$ distance sensitivity.

Observation of either refractive or birefringent Planck space will have a large impact on gravity and related fields.

Acknowledgement

We are gratefull to Reinhard Brinkmann for his support and advices related to the beam setup. One of the authors (V.G.) thanks Stefan Schmitt and Daniel Pitzl for useful discussions.

References

[1] Amsler,C.,*et al.* Review of particle physics. Phys. Lett. B **667** (2008) 1.

[2] G. Amelino-Camelia, J. R. Ellis, N. E. Mavromatos, D. V. Nanopoulos and S. Sarkar, Tests of quantum gravity from observations of gamma-ray bursts, Nature **393**, 763 (1998) [astro-ph/9712103].

[3] Gambini,R. & Pullin,J. Nonstandard optics from quantum spacetime. Phys. Rev. D **59** (1999) 124021.

[4] V. Gharibyan, Testing Planck-Scale Gravity with Accelerators, Phys. Rev. Lett. **109**, 141103 (2012).

[5] R. J. Gleiser, C. N. Kozameh and F. Parisi, On low-energy quantum gravity induced effects on the propagation of light, Class. Quant. Grav. **20**, 4375 (2003) [gr-qc/0304048].

[6] G. Gubitosi, G. Genovese, G. Amelino-Camelia and A. Melchiorri, Planck-scale modifications to Electrodynamics characterized by a space-like symmetry-breaking vector, Phys. Rev. D **82**, 024013 (2010) [arXiv:1003.0878 [gr-qc]].

[7] Hehl,F.W.,Von Der Heyde,P.,Kerlick,G.D. & Nester,J.M. General Relativity with Spin and Torsion: Foundations and Prospects. Rev. Mod. Phys. **48** (1976) 393.

[8] Prasanna,A.R. & Mohanty,S. Photon propagation in torsion background. Gen. Rel. Grav. **41** (2009) 1905.

[9] Myers,R.C. & Pospelov,M. Experimental challenges for quantum gravity. Phys. Rev. Lett. **90** (2003) 211601.

[10] D. A. R. Dalvit, F. D. Mazzitelli and C. Molina-Paris, One loop graviton corrections to Maxwell's equations, Phys. Rev. D **63**, 084023 (2001) [hep-th/0010229].

[11] Ellis,J.R., Mavromatos,N.E. & Nanopoulos,D.V. Derivation of a Vacuum Refractive Index in a Stringy Space-Time Foam Model. Phys. Lett. B **665** (2008) 412.

[12] Dittrich,W. & Gies,H. Light propagation in non-trivial QED vacua. Phys. Rev. D **58** (1998) 025004.

[13] Bombelli,L. & Winkler,O. Comparison of QG induced dispersion with standard physics effects. Class. Quant. Grav. **21** (2004) L89.

[14] Gleiser,R.J. & Kozameh,C.N. Astrophysical limits on quantum gravity motivated birefringence. Phys. Rev. D **64** (2001) 083007.

[15] Stecker,F.W. A New Limit on Planck Scale Lorentz Violation from Gamma-ray Burst Polarization. Astropart. Phys. **35** (2011) 95.

[16] McGlynn,S., Clark,D.J., Dean,A.J., Hanlon,L., McBreen,S., Willis,D. R., McBreen,B., Bird,A.J., Foley,S. Polarisation studies of the prompt gamma-ray emission from GRB 041219a using the spectrometer aboard INTEGRAL. Astronomy & Astrophysics **466** (2007) 895.

[17] D. Heyman, F. Hinteleitner and S. Major, Phys. Rev. D **69**, 105016 (2004).

[18] Gharibyan,V. Possible observation of photon speed energy dependence. Phys. Lett. B **611** (2005) 231.

[19] Ellis,J.R., Mavromatos,N.E. & Nanopoulos,D.V. Probing a Possible Vacuum Refractive Index with Gamma-Ray Telescopes. Phys. Lett. B **674** (2009) 83.

[20] Lipps,F.W.,Tolhoek,H.A. Polarization phenomena of electrons and photons. I: General method and application to Compton scattering. II: Results for Compton scattering. Physica **20** (1954) 85, 385.

[21] McMaster,W.H. Matrix Representation of Polarization. Rev. Mod. Phys. **33** (1961) 8.

[22] Sudarsky,D.,Urrutia,L. & Vucetich,H. New observational bounds to quantum gravity signals. Phys. Rev. Lett. **89**, (2002) 231301.

[23] M. Marx, (ed.), J. Chrin, (ed.), I. Martin, (ed.), (e. .)Muekaphael and V. R. W. Schaa, (ed.), Beam diagnostics and instrumentation for particle accelerators. Proceedings, 10th European Workshop, DIPAC 2011, Hamburg, Germany, May 16-18, 2011, TUPD21, p.350.

[24] Balewski,K.(ed.),Brefeld,W.(ed.), Decking,W.(ed.), Franz,H.(ed.), Rohlsberger,R.(ed.)& Weckert,E.(ed.) PETRA III: A low emittance synchrotron radiation source. Technical design report. DESY-04-035.

[25] Machine Parameters PETRA III (Design Values).
http://hasylab.desy.de/facilities/petra_iii/machine/parameters/

[26] Accelerators at DESY, PETRA III.
http://m.desy.de/accelerators/

[27] Paladin Advanced 355, Modelocked UV Laser.
http://www.coherent.com/downloads/PaladinAdvanced355_DSrevB_0112_2.pdf

[28] T. Aumeyr, G. A. Blair, S. Boogert, G. Boorman, A. Bosco, K. Balewski, E. Elsen and V. Gharibyan *et al.*, A 2-D Laser-wire Scanner at PETRA-III, Conf. Proc. C **100523**, MOPE069 (2010).

[29] J. Chrin, (ed.), M. Marx, (ed.), V. R. W. Schaa, (ed.) and V. Schlott, (ed.), Beam diagnostics and instumentation for particle accelerators. Proceedings, 9th European Workshop, DIPAC 2009, Basel, Switzerland, May 25-27,2009, Villigen, Switzerland: PSI (2009), MOPD20, p.92.

[30] Gamp, Alexander (ed.); Flegel, Ilka (ed.), Accelerators 2011: Highlights and annual report, Hamburg: DESY, 2012 - 87 p ISBN: 978-3-935702-63-8

[31] A. W. Chao, (ed.) and M. Tigner, (ed.), Handbook of accelerator physics and engineering, Singapore, Singapore: World Scientific (2006) 702 p

[32] J. Le Duff, Current And Current Density Limitations In Existing Electron Storage Rings, Nucl. Instrum. Meth. A **239**, 83 (1985).

[33] V. I. Telnov, Scattering Of Electrons On Thermal Radiation Photons In Electron - Positron Storage Rings, Nucl. Instrum. Meth. A **260**, 304 (1987).

[34] B. Dehning, A. C. Melissinos, F. Perrone, C. Rizzo and G. von Holtey, Scattering of high-energy electrons off thermal photons, Phys. Lett. B **249**, 145 (1990).

[35] C. Bernardini, G. F. Corazza, G. Di Giugno, G. Ghigo, R. Querzoli, J. Haissinski, P. Marin and B. Touschek, Lifetime and beam size in a storage ring, Phys. Rev. Lett. **10**, 407 (1963).

[36] R. Klein, R. Thornagel, G. Ulm, T. Mayer and P. Kuske, Beam diagnostics at the BESSY I electron storage ring with Compton backscattered laser photons: Measurement of the electron energy and related quantities, Nucl. Instrum. Meth. A **384**, 293 (1997).

[37] N. Muchnoi, H. J. Schreiber and M. Viti, ILC Beam Energy Measurement by means of Laser Compton Backscattering, Nucl. Instrum. Meth. A **607**, 340 (2009) [arXiv:0812.0925 [physics.ins-det]].

[38] G. Kube, K. Balewski, A. Brenger, H. T. Duhme, V. Gharibyan, J. Klute, K. Knaack and I. Krouptchenkov *et al.*, Overview of the Diagnostics Systems of PETRA III, Conf. Proc. C **0806233**, TUPC111 (2008).

[39] Anthony,P.L.,*et al.* [SLAC E158 Collaboration] Observation of parity nonconservation in Moller scattering. Phys. Rev. Lett. **92** (2004) 181602.

[40] Anthony,P.L.,*et al.* [SLAC E158 Collaboration] Precision measurement of the weak mixing angle in Moller scattering. Phys. Rev. Lett. **95** (2005) 081601.

[41] F. E. Maas [A4 Collaboration], Parity violating electron scattering at the MAMI facility in Mainz, Eur. Phys. J. A **24S2**, 47 (2005).

[42] F. E. Maas [A4 Collaboration], Parity violating electron scattering and strangeness in the nucleon, AIP Conf. Proc. **1056**, 98 (2008).

[43] D. P. Barber, H. D. Bremer, M. Boge, R. Brinkmann, W. Bruckner, C. Buscher, M. Chapman and K. Coulter *et al.*, The HERA polarimeter and the first observation of electron spin polarization at HERA, Nucl. Instrum. Meth. A **329**, 79 (1993).

[44] A. A. Sokolov and I. M. Ternov, On Polarization and spin effects in the theory of synchrotron radiation, Sov. Phys. Dokl. **8**, 1203 (1964) [Dokl. Akad. Nauk Ser. Fiz. **153**, 1052 (1964)] [Phys. Dokl. **8**, 1203 (1964)].